analytical chemistry

Article

pubs.acs.org/ac

Spatially Shaped Laser Pulses for the Simultaneous Detection of Polycyclic Aromatic Hydrocarbons as well as Positive and Negative Inorganic Ions in Single Particle Mass Spectrometry

Julian Schade,[†] Johannes Passig,*[,‡,†] Robert Irsig,[∥,†] Sven Ehlert,[∥] Martin Sklorz,[‡] Thomas Adam,[‡,§] Chunlin Li,[⊥] Yinon Rudich,[⊥] and Ralf Zimmermann[‡,†]

[†]Joint Mass Spectrometry Centre, Chair of Analytical Chemistry, University Rostock, 18059 Rostock, Germany

[‡]Joint Mass Spectrometry Centre, Cooperation Group 'Comprehensive Molecular Analytics' (CMA), Helmholtz Zentrum München, 85764 Neuherberg, Germany

[∥]Photonion GmbH, 19061 Schwerin, Germany

[§]Bundeswehr University Munich, 85577 Neubiberg, Germany

[⊥]Department of Earth and Planetary Sciences, Weizmann Institute of Science, Rehovot 76100, Israel

Supporting Information

ABSTRACT: Polycyclic aromatic hydrocarbons (PAHs) are toxic organic trace components in atmospheric aerosols that have impacts on climate and human health. They are bound to airborne particles and transported over long distances. Observations of their distribution, transport pathways, and degradation are crucial for risk assessment and mitigation. Such estimates would benefit from online detection of PAHs along with analysis of the carrying particles to identify the source. Typically, laser desorption/ionization (LDI) in a bipolar mass spectrometer reveals the inorganic constituents and provides limited molecular information. In contrast, two-step ionization approaches produce detailed PAH mass spectra from individual particles but without the source-specific inorganic composition. Here we report a new technique that yields the single-particle PAH composition along with both positive and negative inorganic ions via LDI. Thus, the complete particle characterization and source apportionment from conventional bipolar LDI-analysis becomes possible, combined with a detailed PAH spectrum for the same particle. The key idea of the method is spatiotemporal matching of the ionization laser pulse to the transient component distribution in the particle plume after laser desorption. The technique is robust and field-deployable with only slightly higher costs and complexity compared to two-step approaches. We demonstrate its capability to reveal the PAH-distribution on different particle types in combustion aerosols and ambient air.

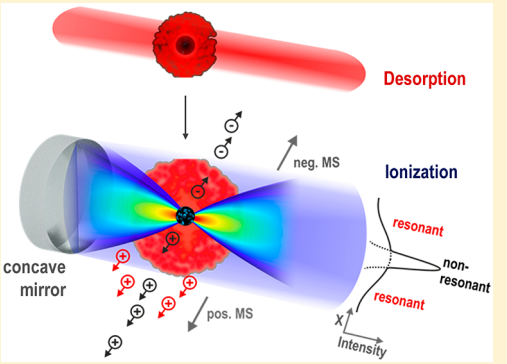

The ubiquitous presence and the persistence of PAHs in the atmosphere is an increasing matter of concern. Some of these byproducts from anthropogenic and natural combustion processes are strong carcinogens.[1,2] As an important fraction of carbonaceous and organic aerosols (OA), PAHs have both direct[3−5] and indirect climate effects, e.g., via photooxidation and interaction with water, thus contributing to the formation of cloud condensation nuclei.[6,7] Despite years of research, little is known about the detailed distribution pathways and the complex interactions with other aerosol components that can modulate the PAH degradation processes.[8−10] For example, coating effects in OA are currently considered to shield PAHs against (photo)oxidation via ozone.[11] Assessment and mitigation strategies require real-time observations and sophisticated source apportionment. Some features in PAH profiles are indicative of specific sources[12,13] but are difficult to measure in real time. Furthermore, the particle's organic and inorganic composition as well as its morphology are key data for a deepened investigation of the PAH chemistry on atmospheric particles. Because the larger PAHs are rapidly adsorbed to the particle phase, the source attribution via inorganic composition and via the PAH profile should complement each other in a single-particle experiment. Single-particle determination of PAHs could also reveal their distribution in an aerosol ensemble. This is a crucial information for health estimates because these species may be concentrated within a small particle subgroup, leading to a high local dose upon deposition in the lung.

A real-time method obtaining the size and chemical information from individual particles is single-particle mass spectrometry (SPMS).[14] Herein particles are introduced into vacuum, sized using laser velocimetry, and finally exposed to an intense UV laser pulse.[15,16] Thus, both positive and negative

Received: May 29, 2019
Accepted: June 28, 2019
Published: June 28, 2019

DOI: 10.1021/acs.analchem.9b02477
Anal. Chem. XXXX, XXX, XXX−XXX

ions are formed by laser desorption/ionization (LDI) and detected in a bipolar MS setup. Common ionization products are cations of metals, salts, or ammonia. Nitrate, sulfate, phosphate, and carbon clusters from organic or elemental carbon (OC, EC) are simultaneously detected in negative mode. Mainly because of matrix effects in LDI ion formation, absolute quantification in terms of mass concentration is difficult in SPMS.[17−19] However, the combined signatures of positive and negative ions together with the particle size often allow a detailed classification and source attribution of many thousand particles in a typical SPMS study.

Most of the numerous particle-bound organic compounds in ambient aerosols[20] are fragmented by the intense LDI laser pulse; thus, organic speciation is limited. Some fragment peaks indicate oxygen-containing molecules or other functional groups as studied with laboratory particles.[21] Important molecular species that are frequently detected in SPMS on ambient aerosols comprise oxalic acid (photooxidation marker),[22,23] methanesulfonate (marine environments),[24] or alkylamines.[25] Also oligomer formation was observed by peak series in negative mode,[26] and the EC/OC content can be determined on a single-particle basis.[27,28] For specific particle matrixes (EC), molecular PAHs are also detectable by LDI-SPMS.[29] However, a substantially improved detection efficiency, yielding detailed PAH spectra from single particles is achieved by two-step ionization methods.[30−33] Herein an IR pulse from a CO_2-laser (wavelength 10.6 μm) heats the particle and desorbs the organic content (laser desorption, LD). Alternatively, the particle impacts a heated rod for thermal desorption (TD).[34,32] After a delay of few microseconds, the molecules in the expanding desorption plume are photoionized by a UV laser pulse. While also single-photon ionization with VUV photons was demonstrated for organic laboratory particles,[35,36] the PAHs can be selectively ionized with much higher sensitivity via resonance-enhanced multiphoton ionization (REMPI).[37] The vaporization prior to photoionization considerably increases the sensitivity, reduces fragmentation and matrix effects, and improves quantification.[38] However, these two-step methods cannot detect the inorganic and refractory components that indicate the type and source of the PAH-carrying particle. Recently, this limitation was overcome by a three-step ionization scheme.[39] However, this approach is technically challenging and it requires a third laser for LDI in addition to the lasers for LD and REMPI. Furthermore, only positive ions can be measured, substantially reducing the LDI-based information compared to conventional bipolar LDI.

Here we present a new approach that combines all three ionization channels for single particles: positive and negative ions from LDI similar to conventional SPMS together with full-fledged mass spectra of PAHs via REMPI. The method utilizes a special laser pulse profile that is matched to the spatial separation of the PAHs from the refractory particle residue, thus inducing LDI and REMPI within a single laser shot. Because only two lasers are required, such as in the two-step approaches, the new technique is easy and robust. It is applicable for existing SPMS setups with moderate modifications. We demonstrate the method's potential for comprehensive chemical characterization and source apportionment with laboratory and real-world particles.

EXPERIMENTAL SECTION

The SPMS instrument is based on two reflectron time-of-flight mass analyzers (Stefan Kaesdorf GmbH) and corresponds to the ATOF-MS technique, such as commercial realizations (LAAPTOF, Aeromegt GmbH, or SPAMS, Hexin Ltd.). Modifications to the previous version[39] comprise the optical setup and the high-voltage supplies as described in the following. After velocimetric sizing, the particles are exposed to a CO_2-laser pulse for efficient desorption by intense IR radiation (10.6 μm, see Figure 1(a)). The central concept of our method is the spatial beam profile of the single ionization laser pulse provided by a KrF-Excimer laser (248 nm). As illustrated in Figure 1(b), the parallel beam intersects the gaseous plume with a rather low intensity (~3 MW/cm^2) for REMPI of the desorbed PAHs. After exiting the vacuum chamber, the laser beam is back-reflected by a concave mirror (f = 150 mm). The beam intersects the plume again, now with a much smaller diameter and hits the particle residue with a high intensity (~2 GW/cm^2) for LDI of the refractory components. An alternative optical setup for the same beam profile is shown in the Supporting Information Figure S1.

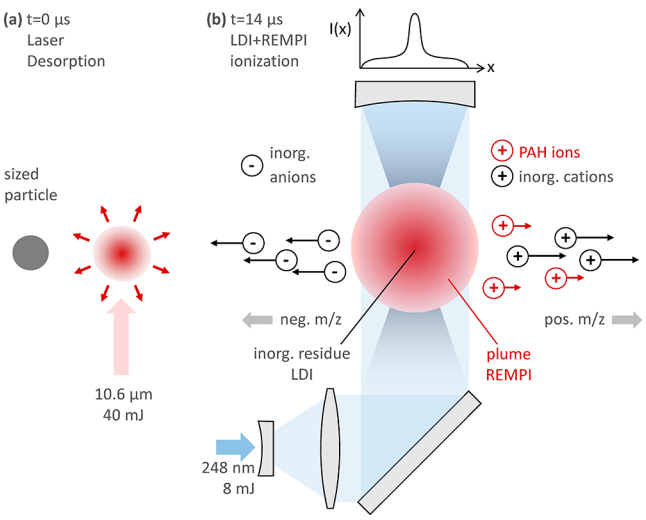

Figure 1. Schematic view of the single-particle approach for simultaneous detection of PAHs along with inorganic cations and anions. (a) The particle is hit by an IR laser pulse for desorption of organics. (b) After 14 μs, the expanding plume (red) is illuminated with a broad UV laser beam (blue) for REMPI of PAHs. The same pulse is reflected and focused on the particle residue (black), ionizing refractory inorganics via LDI with much higher intensity. Note the schematic beam intensity profile at intersection with the particles (top) and the optical parameters in Table 1. Inorganic and PAH cations are detected in one mass analyzer of the bipolar TOF-setup, and inorganic anions in the opposite one.

Both REMPI and LDI are simultaneously induced by the same laser pulse (delay from optical path difference ≈1 ns, <5 ns pulse length) (Table 1). No further ionization laser is required. The ions are extracted after a delay of 0.6 μs, which improves mass resolution and peak quality.[40,41] While anions from LDI are conventionally detected in the negative TOF-tube, the cations from LDI are measured together with the PAH-ions from REMPI in the positive tube. Because all ions are formed and extracted simultaneously, no deconvolution or individual calibration for the LDI- and REMPI-products is required. However, the large dynamic range of LDI-signals is

DOI: 10.1021/acs.analchem.9b02477
Anal. Chem. XXXX, XXX, XXX−XXX

Table 1. Light Sources and Details of the Optical Setup[a]

	velocimetric sizing	laser desorption	REMPI	LDI
light source	2xGCI-050-L, CrystaLaser Inc.	MTL-3 mini-TEA Edinburgh Instruments Ltd.	Photonex Excimer, Photonion GmbH	
wavelength, medium	532 nm, Nd:YAG	10.6 μm, CO_2	248 nm, KrF	
laser intensity @ part. beam, pulse duration	50 mW, continuous wave	0.2 GW/cm^2, 50 ns	3 MW/cm^2, 5 ns	2 GW/cm^2, 5 ns
interaction spot size (mm)	0.4 (Gaussian)	⌀ 1	5 × 10 (Gaussian x flat top)	0.2 × 0.4 (Gaussian x flat top)
pulse energy (mJ)	–	40	8	

[a]The beam parameters were selected to obtain a favorable detection efficiency and mass spectra quality for all types of model particles discussed in this article.

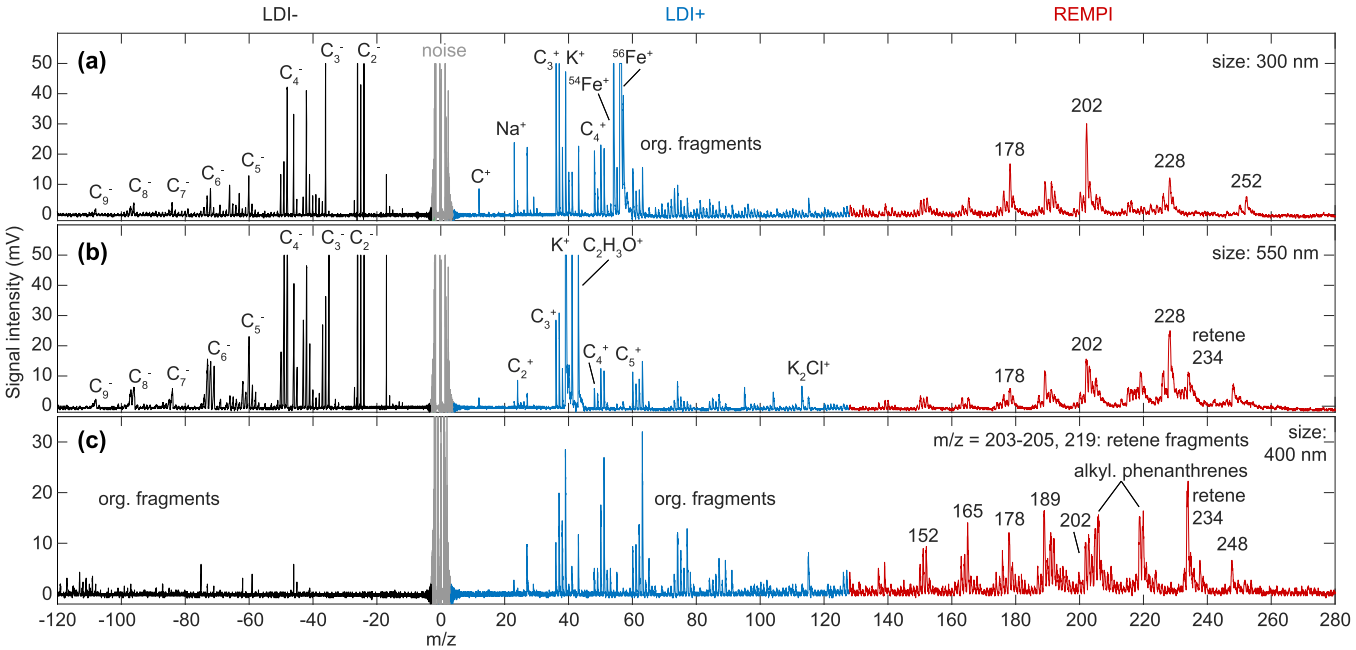

Figure 2. Exemplary mass spectra of single combustion particles, ionized by combined LDI for anions (black), cations (blue), and REMPI for PAHs (red) within the same laser pulse. (a) The LDI spectra from a diesel soot particle reveal EC from soot, iron, and some organic fragments accompanied by mainly unsubstituted PAHs from REMPI. (b) A wood ash particle showing pronounced potassium and soot signatures via LDI. The PAH spectrum exhibits the (coniferous) wood combustion marker retene. (c) Strong positive fragment signals and the presence of at least weak anion fragment signals in the LDI spectrum of a pure organic particle ("tar ball") indicate that it was fully hit by the LDI pulse. The REMPI beam nevertheless yields a detailed PAH spectrum. See Table 2 for a list of PAHs. An example of a particle without PAHs is shown in Figure 4(a). Size distributions of the respective particle classes are provided in Supporting Information Figure S4.

already challenging for a conventional SPMS setup. Here the much weaker signals from the PAHs are measured with the same detector. To achieve high-quality spectra for both ion classes, we attenuate the transmission of the positive flight tube for the lighter LDI ions. This is possible without changing the flight time by detuning a lateral deflection element of the ion optics during the passage of light ions (m/z < 100) and switching it back to optimum transmission before the PAHs (m/z > 120) pass through (2.5 μs after ion extraction, ΔU = 350 V, HV-switches HTS31-03-GSM, rise time 10 ns, Behlke GmbH). Thus, we reduce the sensitivity for LDI cations by a factor of about 20 compared to the PAHs and take full advantage of the system's dynamic range. This allows high-quality spectra with 8-bit digitizers (Agilent Acqiris DP110). A custom LabView software records TOF-spectra and particle sizing signals.

RESULTS AND DISCUSSION

Combustion Particles. The method was designed, tested, and optimized using redispersed combustion particles. Diesel

Table 2. Polycyclic Aromatic Compounds (m/z) That Are Indicated by the REMPI Spectra

	number of C in aliphatic side chain(s)				
PAHs	0	1	2	3	4
naphthalene	128	142	156	170	184
acenaphthylene	152				
phenanthrene, anthracene	178	192	206	220	234 (retene)
pyrene, fluoranthene	202	216	230		
benzanthracene(s), benzphenanthrene(s)	228	242			
benzpyrene(s), benzfluoranthene(s)	252	266			
benz[*ghi*]perylene, indeno(1,2,3)[*c*,*d*]pyrene	276				
dibenzphenanthrene(s), dibenzanthracene(s)	278				
important fragments	115, 139, 165, 189				

DOI: 10.1021/acs.analchem.9b02477
Anal. Chem. XXXX, XXX, XXX−XXX

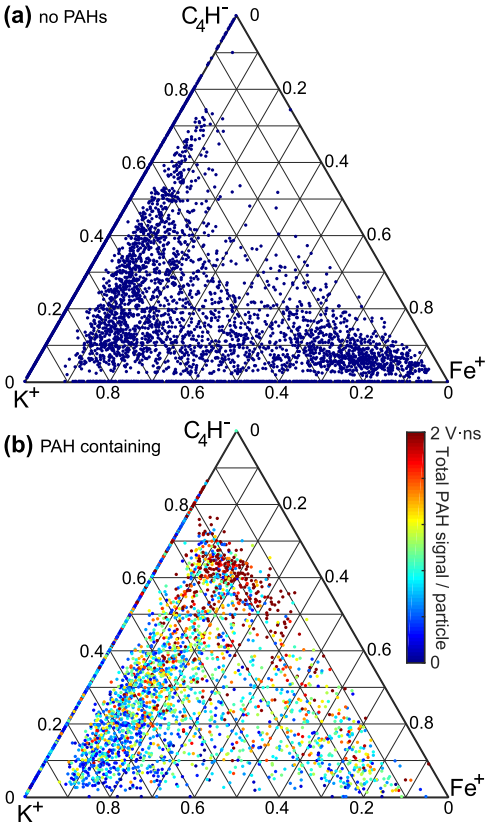

Figure 3. Ternary plots of the single-particle composition with respect to specific inorganic ions from LDI of ambient aerosols. (a) Particles without PAH signatures (n = 19,866) show a cluster with dominant K^+, indicating wood/biomass burning (left corner). Iron-containing particles (right corner) result from several sources, including traffic and coal combustion. Particles almost exclusively showing organic fragments (but no PAHs) are also found (top). (b) PAHs are detected in 5762 particles that resemble some LDI signatures from (a), however with high PAH loads (color-coded) for pure organic particles.

soot particles were extracted from the exhaust pipe of an old diesel van (VW Transporter Typ 3, 1.7 D), milled, and guided into the SPMS instrument with a turntable powder disperser (model 3433 SSPD, TSI Inc.). These particles are well suited for calibration of the optical system, because of their rather uniform PAH content from repeated exposure to flue gases in the exhaust. Optical alignment begins with the LD and REMPI beams, while the concave mirror is blocked. After optimizing the LD-REMPI hit rate (more than 60% for this particle type) and removal of the beam dump, the mirror is adjusted until the additional LDI-spectra appear. About 40% of the sized diesel particles are effectively hit and yield both a PAH spectrum and a bipolar LDI signature. As representatively shown in Figure 2(a), LDI of the soot produces carbon clusters in both positive and negative mode (blue and black). Furthermore, the positive spectra often show a strong iron signal, most likely from the inner surface of the rusty exhaust pipe. Organic fragments are visible for both polarities.[21,42] The PAH signatures (red) reveal contributions from lighter, mainly unsubstituted PAHs, which are typical for diesel emissions; see Table 2 for a list of PAHs and the literature for details on their atmospheric occurrence and sources.[13] Low molecular fractions volatilized before the off-line experiment.

Figure 2(b) shows the spectra of an exemplary particle from coniferous wood combustion in a log wood furnace. As a typical feature of wood/biomass combustion particles, a strong potassium signal appears at m/z = 39 (and 113 for $[K_2Cl]^+$) in the LDI spectrum.[43] The carbon clusters and organic fragments in negative mode resemble the diesel particle spectrum. The REMPI spectrum differs from the diesel particles, showing higher mass fractions and homologous series of alkylated PAHs. Furthermore, the (soft)wood combustion marker retene is clearly visible.[34,44]

An important but not well understood subtype of organic aerosols are homogeneous, spherical particles from wood combustion/smoldering, called "tar balls". Figure 2(c) shows the spectra of a laboratory-generated tar ball (mixed polar and nonpolar phase); see Li et al. for its generation and the scientific background.[4] In contrast to the diesel and wood ash particles, where unsubstituted PAHs dominate the spectrum,

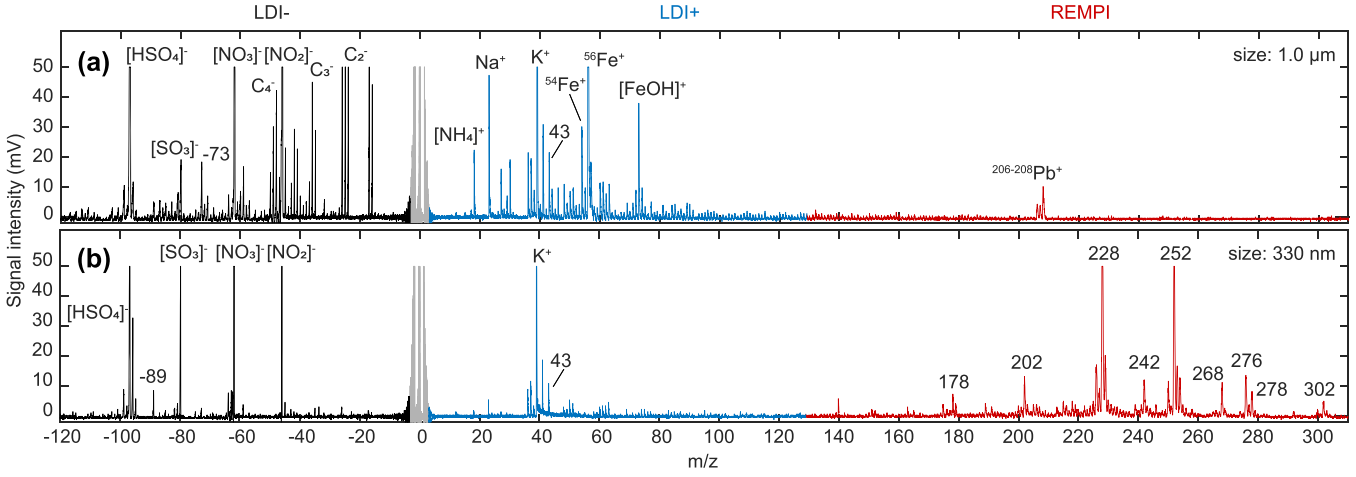

Figure 4. Exemplary mass spectra of ambient air particles. (a) For particles without PAHs, the method yields bipolar LDI mass spectra similar to conventional SPMS. (b) The dominance of m/z = 228 (e.g., chrysene) and m/z = 252 (e.g., benzo(k)fluoranthene) in the PAH spectrum points to coal/wood combustion, in accordance with the strong potassium signal from positive LDI-ions. The negative spectrum reveals important secondary components such as nitrate and sulfate. Photooxidation processes are indicated by the relative strong peak at m/z = 43 ($C_2H_3O^+$, $C_3H_7^+$) and the occurrence of oxalate (m/z = −89).[22,23]

DOI: 10.1021/acs.analchem.9b02477
Anal. Chem. XXXX, XXX, XXX−XXX

also lighter and more alkylated PAHs from incomplete combustion appear in the tar ball REMPI spectrum. Basically, it corresponds to previously measured LD-REMPI mass spectra[4] (no LDI). Both the positive as well as the negative LDI-spectra show almost exclusively organic fragments; see Silva et al. for a detailed discussion on their appearance in LDI.[21]

Method Specific Aspects and Limitations. The new method is different from just a combination of bipolar LDI with LD-REMPI for SPMS. The first important aspect refers to fragmentation. Pure gas-phase REMPI with the parameters of our REMPI-beam is virtually fragment-free.[37] In a LD-REMPI approach, the degree of fragmentation is consequently determined by the internal energy that the particle acquires from laser desorption.[36] In our setup, the intense LDI beam intersects a fraction of the desorbed plume, contributing additional fragment signals to the spectra. This fraction is typically rather small because the plume expands to few millimeters within the 14 μs delay, as measured by moving a narrow REMPI-beam while monitoring the PAH signals of diesel particles. However, in contrast to plume expansion experiments on laboratory particles,[45,36,38] our study deals with complex real-world aerosols, and thus the laser desorption is strongly affected by matrix effects and by the CO_2-laser hit efficiency. Consequently, particles that produce a small plume from inefficient laser desorption, while being fully exposed to the LDI pulse may undergo increased fragmentation, as exemplarily shown in Supporting Information Figure S2. Because the PAHs are very stable molecules and several PAH-specific fragment channels are known (e.g., m/z = 189 from alkylated phenanthrenes[30,34]), the amount of fragmentation and the contribution of aromatics can nevertheless be evaluated.

A further aspect relates to the important class of organic aerosols that are readily identified and characterized by our approach. Basically, it is unlikely that the method fails to detect PAHs if a LDI spectrum is observed, because the broad REMPI beam envelopes the much narrower LDI beam. Moreover, even if the desorption pulse misses the particle completely, at least a small PAH contribution should be detected nevertheless.[29] Vice versa, from the absence of an inorganic signature it is difficult to determine whether the particle is purely organic or whether the smaller LDI beam missed the inorganic residue. The presence of fragment signals alone is not sufficient, because they can also result from the LDI beam traversing the larger plume, as discussed before. However, in case that the positive LDI spectrum shows only organic fragments, the presence of negative ions may indicate that the LDI pulse hit a residual. For example, from 1000 diesel particles revealing PAH spectra and organic fragments, about 250 particles did not produce negative spectra. None of them showed signatures of Na^+ or Fe^+ from LDI; thus, the beam most likely missed possible residues of those particles. In contrast, all particles that produced negative ions also showed at least some signals of the aforementioned cations, even if the anions comprised mostly organic fragments. Furthermore, the dominance of energetically preferred cations and anions such as Na^+ and HSO_4^- over less preferred ones (e.g., NO^+, NO_2^-) result from extensive charge transfer in a dense plume[46] and thus indicates a residue that was hit by the LDI pulse. The complexity of inorganic ion formation and matrix effects[47] should be specifically investigated for our method in later studies.

Ambient Aerosols. To illustrate the application potential of our method, we performed a small online experiment on ambient air in Rostock, Germany (coordinates: 54° 04′ 41.0″ N, 12° 06′ 31.9″ E), during a pollution episode with long-range transported particles from Eastern Europe. The aerosol was concentrated using a virtual impactor device (model 4240, MSP Corp., Shoreview, MN). From the 16th Dec 2018 20:00 to 17th Dec 12:00, a total number of 69 900 particles were detected and sized. The narrow size distribution (see Supporting Information Figure S3) is typical for long-range transported particles[7] and roughly coincides with the highest detection efficiency by laser velocimetry in most SPMS devices.[48] From all sized particles, 36% produced a meaningful mass spectrum from positive LDI and 42% from negative LDI. Thirty percent showed both LDI spectra, and 29% of these particles also exhibited PAHs. Note that negative ion formation in LDI is often affected at humid conditions.[47] However, in our experiment, virtually all particles revealed strong anion signals of both (secondary) sulfate and nitrate from long-range transport.[49] Local contributions were marginal, also due to sparsely populated areas in wind direction. A detailed classification and cluster analysis is beyond the scope of this article, and strong aerosol aging makes source apportionment difficult in this experiment. Nevertheless, the combination of three ionization mechanisms allows interesting insights already at initial overview.

Figure 3(a) indicates the composition of particles without PAH signatures, derived from three ion signals in bipolar LDI. Wood and biomass combustion particles often show dominant K^+ signatures, while fragments are suppressed;[24,50,51] consequently, they appear near the left corner of the ternary plot. Signals from iron are associated with traffic, industrial, or coal-burning emissions.[52] The respective particles form a cluster in the right corner; see Figure 4(a) for an example. Particles in the top corner show a strong anion signal from $[C_4H]^-$, a common negative fragment that is formed by LDI of many aromatic and aliphatic substances.[21] These particles have substantial organic contents of aliphatic hydrocarbons or oxidized/functionalized aromatics rather than pure PAHs. On the contrary, particles with distinct PAH signatures according to Table 2 are shown in Figure 3(b); see also Figure 4(b) for an example. Their LDI-derived composition is roughly comparable to the PAH-free particles, pointing to a rather smooth PAH distribution after long-range transport. However, the highest PAH loads are associated with particles showing nearly pure fragment spectra by LDI (top corner). Organic aerosols (e.g., "brown carbon", "tar balls" etc.) naturally carry large amounts of PAHs. However, the experiment demonstrates that our method yields detailed distributions of the PAHs on several particle classes in real time. Analysis of the ambient PAH spectra itself will be the subject of future publications.

CONCLUSIONS

With the presented method, we exploit the spatial separation of laser-desorbed and refractory components to obtain a full bipolar LDI mass spectrum and a detailed PAH signature of single particles for the first time. Thus, detection and source attribution of PAHs is complemented by the source information on the carrying particle, providing a unique combination of chemical data from individual particles. The technique makes it possible to detect both the carcinogenic PAHs as well as health-relevant metals with the same

DOI: 10.1021/acs.analchem.9b02477
Anal. Chem. XXXX, XXX, XXX−XXX

instrument, while indicating the source and atmospheric aging mechanisms. It reveals the PAH mixing state, a prerequisite to estimate the local dose upon inhalation and to evaluate the health risk. The method works well also for ambient air particles and with manageable complexity. The amount and structure of data from individual particles differs from conventional SPMS; hence, clustering and classification methods would have to be adapted in the future. In conclusion, our approach allows new insights into the single-particle distribution of PAHs, and it will pave the way to a sophisticated understanding of organic aerosols and global air pollution.

■ ASSOCIATED CONTENT

Supporting Information

The Supporting Information is available free of charge on the ACS Publications website at DOI: 10.1021/acs.analchem.9b02477.

An alternative optical setup, further exemplary mass spectra of organic particles showing strong fragmentation from direct LDI, and particle size distributions (PDF)

■ AUTHOR INFORMATION

Corresponding Author

*E-mail: johannes.passig@uni-rostock.de.

ORCID

Johannes Passig: 0000-0002-3876-1716

Yinon Rudich: 0000-0003-3149-0201

Ralf Zimmermann: 0000-0002-6280-3218

Author Contributions

J.P. developed the method and conceived the experiment. J.P., J.S., and R.I. built the instrumental setup with technological assistance from M.S., S.E., T.A., and R.Z. J.S. performed the experiments, analyzed the results, and prepared the figures. C.L. and Y.R. contributed the tar ball aerosols. J.P. wrote the manuscript with input from all authors.

Notes

The authors declare no competing financial interest.

■ ACKNOWLEDGMENTS

The Project was funded by the German Research Foundation (ZI 764/6-1), by the German Federal Ministry for Economic Affairs and Energy (ZF4402101 ZG7), by the Helmholtz International Lab aeroHEALTH (www.aerohealth.eu), and by the Helmholtz Virtual Institute of Complex Molecular Systems in Environmental Health (www.hice-vi.eu). Support by Photonion GmbH, Schwerin, Germany, is gratefully acknowledged. The work is partially supported by a research grant from the Herbert L. Janowsky Lung Cancer Research Fund, Adam Glickman, Eric Gordon, Alex Rotzang, the David M. Polen Charitable Trust, the Benoziyo Endowment Fund for the Advancement of Science, and the Midwest Electron Microscope Project.

■ REFERENCES

(1) Boström, C.-E.; Gerde, P.; Hanberg, A.; Jernström, B.; Johansson, C.; Kyrklund, T.; Rannug, A.; Törnqvist, M.; Victorin, K.; Westerholm, R. *Environ. Health Perspect.* **2002**, *110* (suppl 3), 451−488.

(2) Delgado-Saborit, J. M.; Stark, C.; Harrison, R. M. *Environ. Int.* **2011**, *37*, 383−392.

(3) Chen, Y.; Bond, T. C. *Atmos. Chem. Phys.* **2010**, *10*, 1773−1787.

(4) Li, C.; He, Q.; Schade, J.; Passig, J.; Zimmermann, R.; Meidan, D.; Laskin, A.; Rudich, Y. *Atmos. Chem. Phys.* **2019**, *19*, 139−163.

(5) Samburova, V.; Connolly, J.; Gyawali, M.; Yatavelli, R. L. N.; Watts, A. C.; Chakrabarty, R. K.; Zielinska, B.; Moosmüller, H.; Khlystov, A. *Sci. Total Environ.* **2016**, *568*, 391−401.

(6) IPCC. *Climate Change 2013 - The Physical Science Basis*; Cambridge University Press: Cambridge, 2014.

(7) Seinfeld, J. H.; Pandis, S. N. *Atmospheric chemistry and physics*, 3rd ed.; Wiley: Hoboken, NJ, 2016.

(8) Keyte, I. J.; Harrison, R. M.; Lammel, G. *Chem. Soc. Rev.* **2013**, *42*, 9333−9391.

(9) Pöschl, U.; Shiraiwa, M. *Chem. Rev.* **2015**, *115*, 4440−4475.

(10) Ringuet, J.; Albinet, A.; Leoz-Garziandia, E.; Budzinski, H.; Villenave, E. *Atmos. Environ.* **2012**, *61*, 15−22.

(11) Shrivastava, M.; Lou, S.; Zelenyuk, A.; Easter, R. C.; Corley, R. A.; Thrall, B. D.; Rasch, P. J.; Fast, J. D.; Massey Simonich, S. L.; Shen, H.; Tao, S. *Proc. Natl. Acad. Sci. U.S.A.* **2017**, *114*, 1246−1251.

(12) Czech, H.; Stengel, B.; Adam, T.; Sklorz, M.; Streibel, T.; Zimmermann, R. *Atmos. Environ.* **2017**, *167*, 212−222.

(13) Ravindra, K.; Sokhi, R.; van Grieken, R. *Atmos. Environ.* **2008**, *42*, 2895−2921.

(14) Pratt, K. A.; Prather, K. A. *Mass Spectrom. Rev.* **2012**, *31*, 17−48.

(15) Hinz, K.-P.; Spengler, B. *J. Mass Spectrom.* **2007**, *42*, 843−860.

(16) Murphy, D. M. *Mass Spectrom. Rev.* **2007**, *26*, 150−165.

(17) Gemayel, R.; Temime-Roussel, B.; Hayeck, N.; Gandolfo, A.; Hellebust, S.; Gligorovski, S.; Wortham, H. *Talanta* **2017**, *174*, 715−724.

(18) Gross, D. S.; Gälli, M. E.; Silva, P. J.; Prather, K. A. *Anal. Chem.* **2000**, *72*, 416−422.

(19) Healy, R. M.; Sciare, J.; Poulain, L.; Crippa, M.; Wiedensohler, A.; Prévôt, A. S. H.; Baltensperger, U.; Sarda-Estève, R.; McGuire, M. L.; Jeong, C.-H.; McGillicuddy, E.; O'Connor, I. P.; Sodeau, J. R.; Evans, G. J.; Wenger, J. C. *Atmos. Chem. Phys.* **2013**, *13*, 9479−9496.

(20) Nozière, B.; Kalberer, M.; Claeys, M.; Allan, J.; D'Anna, B.; Decesari, S.; Finessi, E.; Glasius, M.; Grgić, I.; Hamilton, J. F.; Hoffmann, T.; Iinuma, Y.; Jaoui, M.; Kahnt, A.; Kampf, C. J.; Kourtchev, I.; Maenhaut, W.; Marsden, N.; Saarikoski, S.; Schnelle-Kreis, J.; Surratt, J. D.; Szidat, S.; Szmigielski, R.; Wisthaler, A. *Chem. Rev.* **2015**, *115*, 3919−3983.

(21) Silva, P. J.; Prather, K. A. *Anal. Chem.* **2000**, *72*, 3553−3562.

(22) Sullivan, R. C.; Prather, K. A. *Environ. Sci. Technol.* **2007**, *41*, 8062−8069.

(23) Yang, F.; Chen, H.; Wang, X.; Yang, X.; Du, J.; Chen, J. *Atmos. Environ.* **2009**, *43*, 3876−3882.

(24) Arndt, J.; Sciare, J.; Mallet, M.; Roberts, G. C.; Marchand, N.; Sartelet, K.; Sellegri, K.; Dulac, F.; Healy, R. M.; Wenger, J. C. *Atmos. Chem. Phys.* **2017**, *17*, 6975−7001.

(25) Healy, R. M.; Evans, G. J.; Murphy, M.; Sierau, B.; Arndt, J.; McGillicuddy, E.; O'Connor, I. P.; Sodeau, J. R.; Wenger, J. C. *Anal. Bioanal. Chem.* **2015**, *407*, 5899−5909.

(26) Gross, D. S.; Gälli, M. E.; Kalberer, M.; Prevot, A. S. H.; Dommen, J.; Alfarra, M. R.; Duplissy, J.; Gaeggeler, K.; Gascho, A.; Metzger, A.; Baltensperger, U. *Anal. Chem.* **2006**, *78*, 2130−2137.

(27) Ferge, T.; Karg, E.; Schröppel, A.; Coffee, K. R.; Tobias, H. J.; Frank, M.; Gard, E. E.; Zimmermann, R. *Environ. Sci. Technol.* **2006**, *40*, 3327−3335.

(28) Spencer, M. T.; Prather, K. A. *Aerosol Sci. Technol.* **2006**, *40*, 585−594.

(29) Zimmermann, R.; Ferge, T.; Gälli, M.; Karlsson, R. *Rapid Commun. Mass Spectrom.* **2003**, *17*, 851−859.

(30) Bente, M.; Sklorz, M.; Streibel, T.; Zimmermann, R. *Anal. Chem.* **2008**, *80*, 8991−9004.

(31) Morrical, B. D.; Fergenson, D. P.; Prather, K. A. *J. Am. Soc. Mass Spectrom.* **1998**, *9*, 1068−1073.

DOI: 10.1021/acs.analchem.9b02477
Anal. Chem. XXXX, XXX, XXX−XXX

(32) Sykes, D. C.; Woods, E.; Smith, G. D.; Baer, T.; Miller, R. E. *Anal. Chem.* **2002**, *74*, 2048−2052.
(33) Zelenyuk, A.; Imre, D. *Aerosol Sci. Technol.* **2005**, *39*, 554−568.
(34) Bente, M.; Sklorz, M.; Streibel, T.; Zimmermann, R. *Anal. Chem.* **2009**, *81*, 2525−2536.
(35) Hanna, S. J.; Campuzano-Jost, P.; Simpson, E. A.; Robb, D. B.; Burak, I.; Blades, M. W.; Hepburn, J. W.; Bertram, A. K. *Int. J. Mass Spectrom.* **2009**, *279*, 134−146.
(36) Nash, D. G.; Liu, X. F.; Mysak, E. R.; Baer, T. *Int. J. Mass Spectrom.* **2005**, *241*, 89−97.
(37) Gunzer, F.; Krüger, S.; Grotemeyer, J. *Mass Spectrom. Rev.* **2019**, *38*, 202−217.
(38) Woods, E.; Smith, G. D.; Dessiaterik, Y.; Baer, T.; Miller, R. E. *Anal. Chem.* **2001**, *73*, 2317−2322.
(39) Passig, J.; Schade, J.; Oster, M.; Fuchs, M.; Ehlert, S.; Jäger, C.; Sklorz, M.; Zimmermann, R. *Anal. Chem.* **2017**, *89*, 6341−6345.
(40) Li, L.; Liu, L.; Xu, L.; Li, M.; Li, X.; Gao, W.; Huang, Z.; Cheng, P. *J. Am. Soc. Mass Spectrom.* **2018**, *29*, 2105−2109.
(41) Vera, C. C.; Trimborn, A.; Hinz, K.-P.; Spengler, B. *Rapid Commun. Mass Spectrom.* **2005**, *19*, 133−146.
(42) Toner, S. M.; Sodeman, D. A.; Prather, K. A. *Environ. Sci. Technol.* **2006**, *40*, 3912−3921.
(43) Lee, A. K. Y.; Willis, M. D.; Healy, R. M.; Wang, J. M.; Jeong, C.-H.; Wenger, J. C.; Evans, G. J.; Abbatt, J. P. D. *Atmos. Chem. Phys.* **2016**, *16*, 5561−5572.
(44) Shen, G.; Tao, S.; Wei, S.; Zhang, Y.; Wang, R.; Wang, B.; Li, W.; Shen, H.; Huang, Y.; Yang, Y.; Wang, W.; Wang, X.; Simonich, S. L. M. *Environ. Sci. Technol.* **2012**, *46*, 4666−4672.
(45) Cabalo, J.; Zelenyuk, A.; Baer, T.; Miller, R. E. *Aerosol Sci. Technol.* **2000**, *33*, 3−19.
(46) Reinard, M. S.; Johnston, M. V. *J. Am. Soc. Mass Spectrom.* **2008**, *19*, 389−399.
(47) Neubauer, K. R.; Johnston, M. V.; Wexler, A. S. *Atmos. Environ.* **1998**, *32*, 2521−2529.
(48) Marsden, N.; Flynn, M. J.; Taylor, J. W.; Allan, J. D.; Coe, H. *Atmos. Meas. Tech.* **2016**, *9*, 6051−6068.
(49) Dall'Osto, M.; Beddows, D. C. S.; McGillicuddy, E. J.; Esser-Gietl, J. K.; Harrison, R. M.; Wenger, J. C. *Atmospheric Chemistry and Physics* **2016**, *16*, 9693−9710.
(50) Healy, R. M.; Hellebust, S.; Kourtchev, I.; Allanic, A.; O'Connor, I. P.; Bell, J. M.; Healy, D. A.; Sodeau, J. R.; Wenger, J. C. *Atmos. Chem. Phys.* **2010**, *10*, 9593−9613.
(51) Moffet, R. C.; de Foy, B.; Molina, L. T.; Molina, M. J.; Prather, K. A. *Atmos. Chem. Phys.* **2008**, *8*, 4499−4516.
(52) Dall'Osto, M.; Beddows, D. C. S.; Harrison, R. M.; Onat, B. *Environ. Sci. Technol.* **2016**, *50*, 4212−4220.

DOI: 10.1021/acs.analchem.9b02477
Anal. Chem. XXXX, XXX, XXX−XXX